Carboxylation of sulfated cellulose nanocrystals by family AA9 lytic polysaccharide monooxygenases

Cellulose (2023) 30:9331–9347
https://doi.org/10.1007/s10570-023-05440-0

ORIGINAL RESEARCH

Carboxylation of sulfated cellulose nanocrystals by family AA9 lytic polysaccharide monooxygenases

Saül Llàcer Navarro · Monika Tõlgo · Lisbeth Olsson · Tiina Nypelö

Received: 5 December 2022 / Accepted: 7 August 2023 / Published online: 10 September 2023

Abstract Lytic polysaccharide monooxygenases (LPMOs) from the auxiliary activity 9 (AA9) family act on cellulose through an oxidative mechanism that improves cellulose saccharification in concert with other cellulolytic enzymes. Degradation and solubilization of cellulose chains are known to take place when various cellulose hierarchies, fibers, nanofibers, and cellulose nanocrystals (CNCs) are subjected to LPMOs, either alone or in combination with other cellulose acting enzymes. The use of LPMOs to modify and prepare CNCs has been proposed mostly in top-down synthesis from larger hierarchies. Here, we attempted a direct surface modification of CNCs with LPMOs with the aim of investigating the role played by the charged sulfate groups on CNCs. Sulfate half-ester groups are introduced during the preparation of CNCs from cellulose using sulfuric acid. It has been proposed that the charged sulfate groups hinder the binding of enzymes or affinity of charged reactants on the surface and hence reduce enzymatic and chemical reaction efficiency. We demonstrate the modification of commercial sulfated CNCs using a family AA9 LPMO. Conductometric titration and spectrometric characterization of the oxidized particles indicate that carboxylation of up to 10% was possible without degradation of the crystals. Unexpectedly, the carboxyl groups could only be introduced to the crystals containing sulfate groups, while desulfated crystals remained unfunctionalized. This was deemed to be due to that the sulfate groups limit the adsorption of the enzymes and hence modulate the cuts facilitated by the enzymes on the surface. This limits the release of chains from the surface and enables the carboxylation of the insoluble substrate rather than the release of the solubilized chains. This study highlights the importance of analyzing both the solid and soluble reaction products to gain insights into the oxidation mechanism. We demonstrated that 10% functionalization suffices for the use of CNCs in coupling chemistry.

Saül Llàcer Navarro and Monika Tõlgo have contributed equally to this work.

Supplementary Information The online version contains supplementary material available at https://doi.org/10.1007/s10570-023-05440-0.

S. Llàcer Navarro · T. Nypelö
Department of Chemistry and Chemical Engineering, Chalmers University of Technology, 41296 Gothenburg, Sweden

S. Llàcer Navarro · M. Tõlgo · L. Olsson (✉) · T. Nypelö (✉)
Wallenberg Wood Science Center, Chalmers University of Technology, 41296 Gothenburg, Sweden
e-mail: lisbeth.olsson@chalmers.se

T. Nypelö
e-mail: tiina.nypelo@chalmers.se

M. Tõlgo · L. Olsson
Department of Biology and Biological Engineering, Chalmers University of Technology, 41296 Gothenburg, Sweden

Keywords Enzyme · Lytic polysaccharide monooxygenase · LPMO · Cellulose nanocrystal · CNC · Crystalline substrate · Cellulose · Sulfate half-ester groups · Analytics · Amidation

Mathematics Subject Classification MSC code1 · MSC code2

Introduction

The percolation of nanotechnology into wood science led to the discovery of nanocelluloses (Rånby, 1951; Marchessault et al., 1959) that have since been integral materials in the field of cellulose science and technology (Dufresne, 2013). Cellulose nanocrystals (CNCs) are cellulose nanomaterials manufactured by disintegrating cellulose biomass using mineral acids (Habibi et al., 2010). Selective acid hydrolysis of the most accessible cellulose structures leads to the liberation of rod-like crystalline nanoparticles. Hydrolysis using sulfuric acid simultaneously esterifies the particles' surface to carry sulfate half-ester groups (Marchessault et al., 1961; Revol et al., 1992). The sulfate half-ester groups provide a negative charge to the particles. The charge is a requisite for colloidal stability and serves in medical use, for example, in heparin-mimicking anticoagulants (Ehmann et al., 2014).

The carboxyl groups on CNCs enable their use in coupling chemistry (Akhlaghi et al., 2013; Akhlaghi et al., 2014). Carboxyl groups are introduced to cellulose via 2,2,6,6-tetramethyl piperidine-1-oxyl through C6 (TEMPO)-mediated oxidation (Isogai et al., 2011), via esterification using weak acids (Ji et al., 2019) and even by using ozone to oxidize aldehyde groups that have been introduced to the positions C2 and C3 (Nypelö et al., 2018). Surgicel® (branded by Johnson & Johnson), Oxycel® (Becton Dickinson) and Traumacel® (Bioster a.s.) are commercial oxidized medical cellulose products (Zhang et al., 2020). Although carboxylation is efficiently performed using chemical reaction pathways, there is a need for reagents that have a lower environmental impact and are non-toxic, especially when the product is targeted for use in medicine.

Lytic polysaccharide monooxygenases (LPMOs) are mono-copper carbohydrate active enzymes that were discovered in 2010 (Vaaje-Kolstad et al., 2010). Depending on their regiospecificity, LPMOs cleave various polysaccharides by oxidizing the substrate at C1 and/or C4 positions (Vu et al., 2014; Wang et al., 2018). In addition, indications of C6 oxidation have been presented (Sun et al., 2022; Chen et al., 2018). Repeated attacks in localized areas or close to the chain end lead to the peeling of soluble oligosaccharides from the surface (Courtade et al., 2018; Solhi et al., 2022). The reaction products from C1-oxidizing LPMOs are lactones in equilibrium with aldonic acids (Fig. 1a) and the reaction products from C4-oxidation are 4-keto sugars in equilibrium with gemdiols. For LPMO catalysis, Cu(II) in the LPMO active site must be reduced to Cu(I) by an electron donor and the enzyme also requires an oxygen-containing co-substrate (O_2 and/or H_2O_2) for activity (Vaaje-Kolstad et al., 2010; Quinlan et al., 2011; Bissaro et al., 2017). Family AA9 LPMOs (abbreviated as AA9s or LPMO9s, according to the CAZy (Carbohydrate-Active EnZYmes) database (Drula et al. , 2022)) are LPMOs of fungal origin, and they have so far shown activity on cellulose, various hemicelluloses, and the respective oligomers (Agger et al., 2014; Frommhagen et al., 2015; Bennati-Granier et al., 2015; Hüttner et al., 2019; Tõlgo et al., 2022). Carbohydrate-binding modules (CBM) are non-catalytic enzyme domains that promote enzyme binding onto a substrate and are connected to the catalytic domains via a linker. Cellulose-binding CBMs (e.g. CBM1 and CBM2) have proven to be beneficial in LPMO binding on the cellulose substrate and in localized degradation by LPMOs (Courtade et al., 2018; Chalak et al., 2019; Sun et al., 2022). Enzymes within the same family, such as the LPMO9s, differ biochemically, for example in their substrate preference, modularity (with or without CBM), regioselectivity and reaction kinetics (Frandsen et al., 2021; Petrović et al., 2019; Tõlgo et al., 2022). LPMO9s are industrially interesting because of their ability to boost cellulolytic activities in commercial lignocellulolytic cocktails. Owing to their relatively flat active site and powerful oxidative chemistry, LPMOs can create nicks on otherwise crystalline and recalcitrant polysaccharides which creates binding sites for hydrolytic enzymes in lignocellulolytic cocktails and results in an increase in saccharification yields of various substrates (Chylenski et al., 2019). However, proofs of concept for other applications have also emerged. LPMO9s (alone or in combination with cellulases

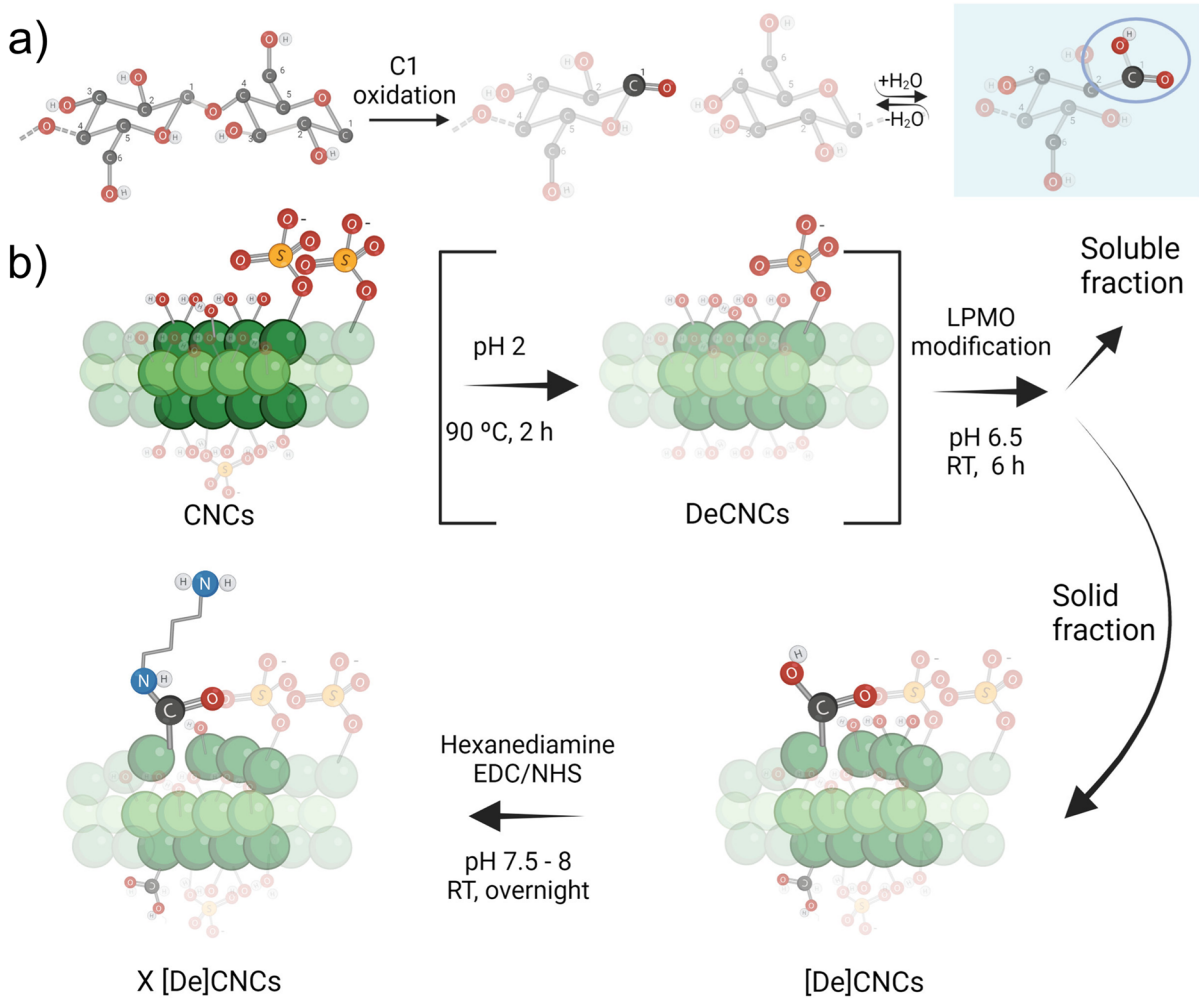

Fig. 1 **a** The mechanism of formation of the C1-oxidized LPMO reaction products on cellulose; on of the products is a lactone in equilibrium with its hydrated aldonic acid form. **b** Schematic presentation of CNCs carrying sulfate half-ester groups, their desulfation, the LPMO treatment of sulfated (CNC) or desulfated (DeCNC) cellulose substrates to carry carboxyl groups, and amidation of the solid product. The soluble fraction would be composed of oxidized and non-oxidized oligosaccharides, however, here the focus was on the analysis of oxidized products as evidence of LPMO activity

and xylanases) have been demonstrated to produce and oxidize cellulose nanomaterials (Villares et al., 2017; Hu et al., 2018; Moreau et al., 2019; Koskela et al., 2019; Karnaouri et al., 2020; Koskela et al., 2021; Muraleedharan et al., 2021; Rossi et al., 2021; Marjamaa et al., 2022; Magri et al., 2022; Chorozian et al., 2022). In addition, a family AA10 cellulose-active LPMO of bacterial origin has been used to carboxylate cellulose fibers and nanocrystals (Solhi et al., 2022). The use of LPMOs is relevant from an industrial lignocellulosic biorefinery perspective as mild and sustainable enzyme-based processes can be used as alternatives to the current chemical and mechanical reaction pathways.

The effect of sulfate half-ester groups on the activities of LPMO9s has been investigated by analyzing the soluble and insoluble oxidized products (Karnaouri et al., 2020; Muraleedharan et al., 2021). Eibinger et al. (2017) showed using atomic force microscopy (AFM) that *Nc*LPMO9F (no CBM1) binds on sulfated CNCs. Karnaouri et al. (2020) showed increased carbonyl and carboxyl group contents on sulfated tunicate CNC when the substrate was LPMO pre-treated or post-modified using a C1/C4-oxidizing

LPMO9 (*Mt*LPMO9H). In contrast, Solhi et al. (2022) showed that functionalization by a specific family AA10 LPMO (*Cfla*LPMO10A) is strongly inhibited by the sulfate half-ester groups. Muraleedharan et al. (2021) concluded that carboxylation by LPMO9s (*Mt*LPMO9H and *Pc*LPMO9D) does not increase carboxyl group content on sulfated CNCs. A similar inhibiting effect on hydrolysis has been seen when hydrolyzing sulfated cellulose with a cellulase mixture from *Trichoderma reesei* (Jiang et al., 2013).

Although there are published works regarding the LPMOs acting on nanocellulose, the ones that deal with the retardation of reactivity stemming from the abundant sulfate ester groups are only a few and sometimes contradicting. The mechanism of how the LPMOs modify the solid crystalline cellulose substrates containing bulky charged groups appears still far from being elucidated and we wish to contribute to this endeavor. We provide a comparison of the functionalization efficiencies of sulfated and desulfated CNCs by an LPMO9. Since commercial CNCs typically contain sulfate half-ester groups, such comparison is a necessity to facilitate their enzymatic modification route. The surface charge that the sulfate groups bring is expected to interfere with the enzyme adsorption onto the solid substrate. The sulfate groups have been shown to prevent the action of a negatively charged chemical oxidant, sodium periodate, via electrosteric repulsion (Llàcer Navarro et al., 2021). We hypothesize that the CNCs will be enzymatically modified, but we also anticipate that there will be a maximum degree of surface functionalization that can be reached due to the limitation posed by the sulfate groups. To test this hypothesis, we employ a previously characterized C1-oxidizing LPMO from *Thermothielavioides terrestris* (*Tt*LPMO9G) (Tõlgo et al., 2022) from the AA9 family to modify sulfated and nonsulfated cellulose nanocrystals. *Tt*LPMO9G contains a C1-oxidizing LPMO9 catalytic domain appended to a CBM1. *Tt*LPMO9G has been shown to have a high specific activity on various cellulosic substrates (Tõlgo et al., 2022). In addition, it was possible to produce this enzyme in sufficient yields on a laboratory scale which is a prerequisite for using it for modifying cellulose. Here, we apply an analysis of both soluble and insoluble products by chromatography and conductometric titration to elucidate the functionalization with respect to where the oxidations are located (on solubilized or on the solid products). The products of the enzymatic modification are analyzed using dynamic light scattering (DLS) for determining the z-average, using zeta-potential for determining colloidal stability, elemental composition, attenuated total reflectance Fourier-transform infrared (ATR-FTIR) spectroscopy, x-ray photoelectron spectroscopy (XPS) and titration to quantify the degree of modification, x-ray diffraction (XRD) to quantify the crystallinity of the CNCs, and AFM to quantify particle dimensions. Moreover, the product of the enzymatic modification is used in coupling chemistry amidation to provide a demonstration of its use in engineered materials.

Experimental

Materials

*Tt*LPMO9G (UniProt ID G2QZK6) was cloned, produced, purified, and stored as described in our earlier work (Tõlgo et al., 2022). CNCs were purchased from Celluforce (Canada). Hexane-1,6-diamine, ascorbic acid (AscA), KCl, HCl, *N*-(3-dimethylaminopropyl)-*N*-ethylcarbodiimide hydrochloride (EDC), *N*-hydroxysuccinimide (NHS), NaOH and BisTris were purchased from Sigma-Aldrich (Sweden) and spectrapore membrane with a cut-off of 12,000–14,000 g mol^{-1} was purchased from VWR (Sweden).

Protonation and desulfation of CNCs

CNCs were dispersed in water as received and protonated by adding HCl until pH value 2 was reached, which is below the pK_a (2.46) of the sulfate half-ester group (Wang et al., 2011). Then the suspensions were dialyzed with the spectrapore membrane until the pH of the dialysate reached the neutral pH of the deionized water used for the dialysis to remove the excess ions. The protonated CNCs are referred to as CNCs.

The sulfate group content was lowered via an acid-catalyzed technique by adding 12 M HCl to a 5 wt% CNC dispersion to obtain an acid concentration of 1.8 M (Fig. 1b). The suspension was heated to 90 °C and stirred with reflux for 2 h. The suspension was then dialyzed against deionized water. The desulfated CNCs are referred to as DeCNCs.

Assessment of *Tt*LPMO9G activity on CNCs

The activity of the LPMO on the cellulose substrates was determined in triplicate using 100 μL reaction volume in 1.5 mL Eppendorf tubes for 16 h reaction time. The LPMO was incubated on ice with a 0.5 eqm amount of $CuSO_4$ for a minimum of 30 min before being used in the reactions. The reactions contained 1 μM *Tt*LPMO9G, 0.4% (w/v) substrate and 50 mM BisTris–HCl, pH 6.5. After mixing, the reductant AscA was added to initiate the reactions in 1 mM final concentration. In control reactions (no reductant, NR), the reductant was replaced by ultrapure water. In other control reactions, the enzyme was replaced with the respective amount of $CuSO_4$ (these reactions did not show any product generation and are not shown). All reactions were incubated for 16 h at 40 °C and 1000 rpm (orbital shaking). The reactions were stopped by boiling for 15 min after which they were filtered using a 0.45 μm membrane plate filter and a vacuum manifold. The filtrates were stored at −20 °C for further analysis.

CNC and DeCNC modification using *Tt*LPMO9G

The LPMO treatment (Fig. 1b) of the cellulose substrates was performed using 104 mL of 2.6 wt% of CNC or DeCNC suspension in a 50 mM BisTris–HCl buffer at pH 6.5 and room temperature with constant stirring (400 rpm) in a 100 mL round flask. The flask was covered with Parafilm with punched holes to allow aeration. The enzyme concentration was 0.9 μM and the concentration of AscA that was used as a reductant was 1 mM. The *Tt*LPMO9G was incubated with a 0.5 eqm amount of $CuSO_4$ on ice for a minimum of 30 min prior to the start of the reactions. AscA was added last to initiate the reaction. The cellulose suspensions were reacted for 6 h and aliquots were taken at 2, 4 and 6 h. The enzymatic reaction was stopped by heating the suspension to 100 °C for 10 min and decreasing the pH to 2. The enzymatically modified cellulose suspensions were purified by dialysis against deionized water. Control reactions were performed without the reductant (NR) and without the LPMO and no $CuSO_4$ (NE) in otherwise equivalent conditions.

Coupling chemistry

The following procedure is an adaptation from Arcot et al. (2014). The LPMO-modified cellulose substrates and the NE control were used for the amidation reaction (Fig. 1b). NHS and EDC in a molar ratio of 1:50 were added to 2 mg ml^{-1} CNC or DeCNC suspension. KCl was then added to a final concentration of 1 M in KCl in suspension. Once the ionic strength of the reaction mixture was increased by KCl, a solution of hexane-1,6-diamine was added so that the resulting reaction mixture had a 1.5:2 hexane-1,6-diamine to carboxyl group content molar ratio. The molar ratio between the hexane-1,6-diamine and the NHS was 1:1. Following the addition of the amine, the reaction mixture was adjusted to pH 9.2 then sonicated and left to stir overnight. The product was dialyzed against deionized water and stored at 4 °C. A prefix X is added to the identifiers of CNCs and DeCNCs to indicate amidation.

High-performance anion exchange chromatography with pulsed amperometric detection (HPAEC-PAD)

HPAEC-PAD was used for the analysis of oxidized soluble products released by the LPMO from the CNC and DeCNC substrates. An ICS-5000 instrument with Carbopac PA200 analytical (3 × 250 mm) and Carbopac PA200 guard column (3 × 50 mm) was used (all Dionex, USA). The soluble product solutions were diluted four-fold in ultrapure water prior to analysis, and 10 μL of the solutions were injected into the columns. The analysis method described by Tõlgo et al. (2022) was used. The analysis was done in duplicate or triplicate, and only the representative single chromatogram is shown for when the chromatograms looked similar. The Glc2-6ox standard was prepared according to Tõlgo et al. (2022) except that cellohexaose was included in the preparation. The standard was diluted ten-fold in ultrapure water prior to HPAEC-PAD analysis. Where semi-quantification was used for the oxidized cello-oligosaccharides, the peak areas of the Glc2-6ox peaks were identified using Chromeleon software and multiplied by the dilution factor, and the relevant peak areas were summed up and compared on a relative basis.

Conductometric titration

Conductometric titration was performed to quantify the carboxyl group content of the solid substrate (i.e., of CNCs and DeCNCs). Protonated and dialyzed cellulose suspensions were diluted with ultrapure water, and HCl and NaCl were added in order to be able to identify two equivalence points and to increase the conductivity to a measurable range, respectively (Foster et al., 2018). Titration was performed under constant stirring using 0.01 M NaOH and a 665 Dosimat titrator coupled to a conductometer and controlled by a python script. The equivalence points were identified by analysis using Matlab: The first equivalence point was taken as an indication of neutralization of the strong acid groups ($-OSO_3H$), and the second equivalence point was of the weak acid groups ($-COOH$). The equivalent points were calculated as the intersections of the linear regressions with an $R^2 > 0.995$ of strong acid, weak acid plateau, and excess of the NaOH regions. The conductivity at each point was calculated from the conductivity measured, Conductivity_m, the initial volume (V_i) of the suspension, and the volume of NaOH (V_{NaOH}) according to Eq. (1).

$$\text{Conductivity} = \text{Conductivity}_m \times \left(\frac{V_i + V_{NaOH}}{V_i} \right) \quad (1)$$

The concentration of the NaOH was standardized using potassium hydrogen phthalate, which was first dried in an oven.

Zeta-potential and z-average

The zeta-potential and z-average, via DLS, of the suspensions were determined using DTS 1070 cuvettes with Zetasizer Nano (Malvern, UK) equipment at 25.0 ± 0.1 °C and in pH 6 using 0.25 wt% cellulose suspension (Foster et al., 2018). The suspensions were sonicated and filtered using a PVDF filter with a 0.45 μm pore size prior to the measurement. The data were analyzed using Malvern Zetasizer Software v7.13. The zeta-potential was calculated as the average of 6 measurements, where each measurement comprised 60 to 150 sub-runs (Bhattacharjee, 2016). A pH 6 was chosen as both, the strong acid, sulfate half-ester groups ($-OSO_3-$ pKa ~ 2), and the weak acid, carboxylic acid groups ($-COO-$ pKa ~ 4.5), are deprotonated (Delepierre et al., 2021). The refractive index for the particles was set to 1.4701.

Attenuated total reflectance Fourier-transform infrared spectroscopy

ATR-FTIR spectra were recorded using a spectrometer (Perkin-Elmer, USA) and films that had been prepared using the cellulose suspensions that were drop-casted on a support and allowed to dry. The spectra were processed with the Spectrum software (Perkin-Elmer, USA). ATR correction was applied and the spectra were normalized to the highest peak (1030 cm^{-1}).

X-ray diffraction (XRD)

XRD spectrograms were acquired between 5° and 70° 2θ on a Bruker D8 Discover diffractometer (USA) in a θ–2θ configuration, equipped with a Cu tube x-ray source and an Eiger2 R 500K 2D detector set to 1D mode. Dried suspensions were mounted on a Si single-crystal zero-background holder. Data acquisition time was set to 20 min, at 0.02° increment and 0.4 s exposure per step. The motorized divergence slit on the incoming beam side was set to 0.2 mm, and an air scattering shield was placed 3 mm above the sample. Samples were rotated at 10 rpm. The background signal of the diffractograms was fitted to a second-degree polynomial and subtracted. The diffractograms were then deconvoluted to Voigt functions using OriginPro (2022). The crystallinity was calculated using the crystalline areas and the amorphous area located approximately at an angle of 2θ of 18°. The crystalline areas were composed of the following peaks: ($1\bar{1}0$), (110), (102), (200), and (004) (French , 2014). An example of deconvolution is shown in Supporting Information Fig. S1.

Atomic force microscopy

Semi-contact mode AFM (NTEGRA, NT-MDT, Russia) with Tap300AI-G tips (BudgetSensors, Bulgaria) was used for imaging of the topography of CNCs and DeCNCs spin coated using SPIN 150 (SPS-Europe, Netherlands) on silicon wafers (Siegert Wafers, Germany). Frame sizes of 5 × 5 μm were recorded. At least 50 potentially single CNCs and DeCNCs for

each specimen were captured in a frame and their height profiles were extracted using Gwyddion 2.56 software. The data processing prior to height profile extraction consisted of removing polynomial backgrounds and aligning the rows. The profiles were baseline corrected using polynomial fitting. The diameter of the particles was calculated from the height profiles.

Sulfur and nitrogen content determination

Elemental analysis was performed by Mikrolab Kolbe (Germany). XPS analysis was performed using a PHI 5000 VersaProbe III Scanning XPS Microprobe at an angle of 45°.

Results and discussion

Composition of CNCs

The sulfur content was determined to quantify the number of sulfate half-ester groups to verify that desulfation took place. CNC NR contained 0.66 ± 0.01 wt% sulfur and DeCNC NR contained 0.07 ± 0.01 wt%.

Release of soluble products by *Tt*LPMO9G on CNCs and DeCNCs

*Tt*LPMO9G had not been tested on any CNC substrates prior to the current study. Therefore, the solubilized product of the *Tt*LPMO9G catalyzed oxidation was analyzed as a probe that the LPMO was active on both CNCs and DeCNCs. It was found that *Tt*LPMO9G was active on both substrates, producing oxidized cellooligos with a degree of polymerization 2-6, denoted as Glc2-6ox (Fig. 2a). Quantification of Glc2-6ox peak areas of each reaction indicated that 27% less oxidized cellooligosaccharides were released by the LPMO from the CNCs than from the DeCNCs, displaying a higher amount of soluble products on the DeCNC substrate (Fig. 2b).

Solhi et al. (2022) reported that the solubilized fraction of cellulose nanocrystals modified with *Cfla*LPMO10A was less than 2 μM from CNC while the solubilized fraction found from the non-sulfated CNCs (comparable to the DeCNCs) was 8 μM when a similar LPMO concentration, as applied here, was used. Solhi et al. (2022) demonstrated that the solubilized fraction content of the non-sulfated reaction was approximately fivefold higher than that of the CNC reaction, displaying a much larger difference between the two cellulose substrates than was demonstrated in the current work. Magri et al. (2022) used three C1-oxidizing LPMO9s on sulfated CNCs among which only one (*Mt*LPMO9A) produced soluble products. Furthermore, at a higher concentration of CNCs (6.5 wt%), the amount of soluble fraction was amplified, and at this CNC concentration, the other two C1-oxidizing LPMOs (*Pc*LPMO9D and *Mt*LPMO9D) also produced soluble products.

Carboxyl group content of CNCs and DeCNCs

The carboxyl group content was determined on the solid reaction products (i.e., on CNCs and DeCNCs) to quantify the LPMO's ability to oxidize the cellulose substrates (Fig. 3). The carboxyl group content of CNCs after 6 h of LPMO oxidation was 0.22 ± 0.00 mmol/g, which was higher than the carboxyl group content of the controls. The carboxyl group content of the NE and NR controls was 0.19 ± 0.01 mmol/g and 0.20 ± 0.00 mmol/g, respectively. The carboxyl group content of CNCs after 6 h modification by LPMO was 10 % higher than the content of the NR control. CNC 6 h reaction was statistically different to the 2 and 4 h reactions (Supporting Information Table S1).

The carboxyl group content of the DeCNCs after 6 h of LPMO oxidation was 0.06 ± 0.01 mmol/g, which was not statistically different from the value of the NR control that was 0.05 ± 0.00 mmol/g (Supporting Information Table S1). However, the NE control carboxyl group content was 0.07 ± 0.02 mmol/g and was statistically different from the content in the other DeCNC suspensions.

Detection of carboxyl groups on CNC NE and CNC NR is a peculiar matter. The CNCs should not intrinsically contain the considerable amount of carboxyl groups that were measured by conductometric titration. Also, the acid catalyzed desulfation should lead to the removal of sulfate groups (Jiang et al., 2010; Llàcer Navarro et al., 2021) without the introduction or removal of other functionalities. Differentiation of the sulfate and carboxyl groups has been reported to be challenging when the concentration of the latter increases affecting the dissociation constants since the determination of the first equivalence point

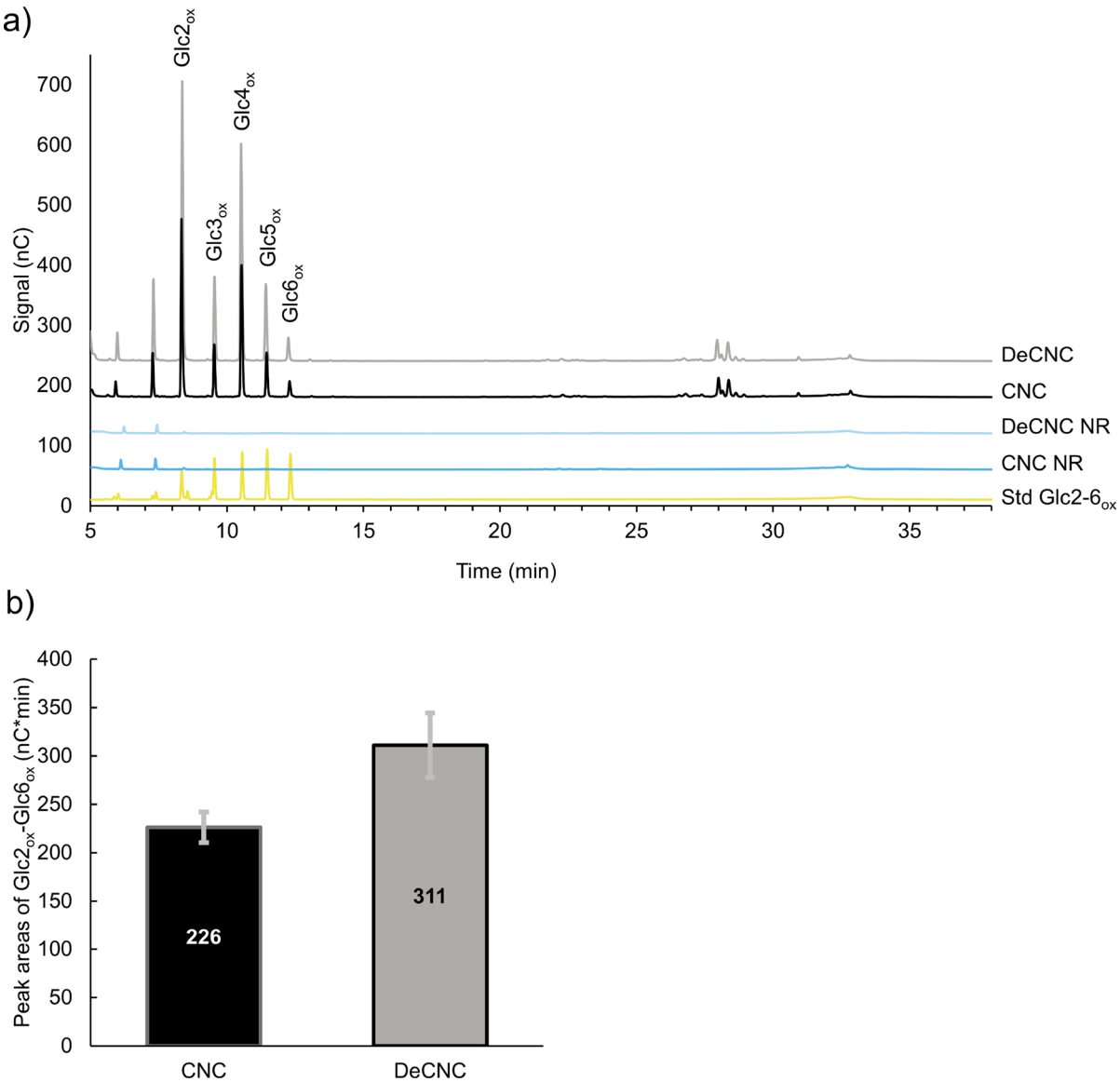

Fig. 2 **a** HPAEC-PAD chromatograms showing the released soluble LPMO reaction products (Glc2ox-Glc6ox) on CNC and DeCNC and **b** their semi-quantification based on the summed peak areas. All reactions were run in 100 μL, at pH 6.5 and 40 °C with 1 μM LPMO and 0.4% (w/v) substrate using 1 mM AscA as the reductant to activate the LPMO (added at time zero to start the reaction). In the control reactions, the reductant was replaced with water (denoted NR, no reductant). The error bars represent the standard deviation of three independent reactions. A single representative chromatogram out of the triplicate analysis is shown for clarity

is obscured (Fraschini et al., 2017). If the amount of sulfur does not change, the effect of the sulfates on the titration should not vary and thus the values of the carboxyl groups between the CNCs can be compared. Moreover, subtracting the values of the NR controls at the different cellulose substrates and using them as baselines did not change the results of the statistical analysis.

Solhi et al. (2022) modified sulfated CNCs with 1 μM *Cfla*LPMO10A and observed an increase of 2% in the total acid content with the modification. Thus, the total amount of acid groups was lower than the

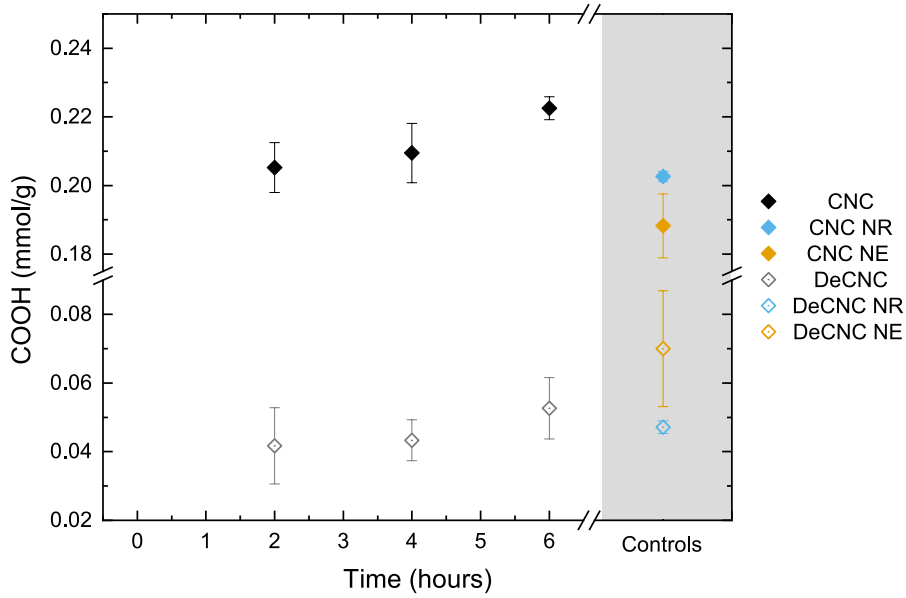

Fig. 3 Carboxyl group content determined using conductometric titration, presented with respect to the reaction time for CNCs (◆) and DeCNCs (◇). The values are an average of at least three repetitions. Controls of CNCs and DeCNCs exposed to the reaction without reductant (NR) and without LPMOs (NE) for 6 h are shown

10% increase in carboxyl group content achieved in the present work (a similar LPMO concentration was used). However, Solhi et al. (2022) performed LPMO oxidation of CNCs that did not contain sulfate groups (and were comparable to DeCNCs), the LPMO oxidation increased the total acid content detected on the surface of the non-sulfated CNC by 80%. That is contradictory to our finding that the DeCNC carboxyl group content was not altered following the LPMO treatment. Since Solhi et al. (2022) determined the total acid content that included the sulfate groups, a direct comparison with our results is not possible. Muraleedharan et al. (2021) found that non-sulfated cellulose substrates (comparable to DeCNC) were more oxidized than sulfated substrates using *Pc*LPMO9D.

The approach of producing cellulose nanomaterials using LPMO oxidation of cellulose hierarchies has been applied to prepare carboxylated CNCs from microcrystalline cellulose with C1-oxidizing *Nc*LPMO9E that has a CBM1 (Koskela et al., 2021). The carboxylated CNC product contained a higher carboxyl group content than in our work, at 0.40 ± 0.07 mmol/g. In the same work, the use of *Nc*LPMO9F (no CBM1) introduced an even higher carboxyl group content on the surface of CNCs, at 0.70 ± 0.09 mmol/g (Koskela et al., 2021). However, the starting material was non-sulfated microcrystalline cellulose instead of CNCs. Because the LMPOs in the current work and within the work of Koskela et al. (2021) had different catalytic and binding domains, it is not possible to draw conclusions on the role of CBM1s on the carboxylation of the surfaces of CNCs. In addition, Karnaouri et al. (2020) showed that post-treatment with *Mt*LPMO9H increased oxidized groups on all three of their tested sulfated tunicin nanocrystal materials.

Comparing the solubilized (Fig. 2) and solid products (Fig. 3) gives an indication that the enzyme action on CNCs led to a lower solubilized product content but a higher degree of functionalization on the solid substrate than the DeCNCs. The sulfate half-ester groups have been suggested to hinder the adsorption of the enzyme on the solid substrate which may limit the probability that the same cellulose chain is cut multiple times at internal positions that are a few anhydroglucose units apart as the proximity of cut sites would enable the liberation of short chains that are soluble (Courtade et al. , 2018). Solubilized products are also released when the enzymes cut close to chain ends, and sulfate groups can possibly also hinder productive enzyme binding in those areas. In summary, it is plausible that the sulfate half-ester groups prevent solubilization. CBM-containing enzymes have been shown to perform localized oxidation (Courtade et al., 2018) that could lead to more solubilized products forming, which in our work might have been impeded by the sulfate groups.

However, the enzyme action on the DeCNC might have led to the solubilization of carboxyl groups higher or equal to the number of the carboxyl groups that the LPMO added and hence lead to a net neutral change in the charge content. This was reported by Muraleedharan et al. (2021). The difference in findings depending on the fraction analyzed highlights the importance of analyzing both solid and solubilized products. Solhi et al. (2022) analyzed both solubilized and solid products, in which the sulfated CNCs were not modified and did not release soluble fractions; the CNCs that did not contain sulfate groups (comparable to the DeCNCs) were both modified and had more solubilized fraction.

FTIR spectroscopy was used to complement the titration analysis and confirm the presence of carboxyl groups on the cellulose substrates (Fig. 4). The band intensity at 1745–1735 cm^{-1}, which is attributed to the C = O stretching associated with carboxyl groups increased with the modification of CNCs, indicating that these groups were indeed introduced through the LPMO catalyzed oxidation. The band was not detected in this region for the DeCNCs (Fig. 4), indicating that the number of carboxyl groups did not increase with the LPMO treatment. The band associated with carboxyl groups was also observed in the spectra of the gluconolactone that is shown for reference (Fig. 4). The FTIR spectra displayed the absorbance bands of C–O stretching (1170–1050 cm^{-1}), C–H bending (1450–1300 cm^{-1}), and O–C–H in-plane bending vibrations at 1430 cm^{-1} that are characteristic of cellulose. The 1635 cm^{-1} band was attributed to the H–O–H bending vibration and hydrogen bonded hydroxyl groups along with absorbed water. Two absorbance bands were attributed to the presence of the sulfate half-ester groups on the cellulose substrates. One of the bands observed at 1250 cm^{-1} was due to asymmetrical S = O vibration (Gu et al., 2010), which can not be isolated in Fig. 4 due to the overlap with other bands. The other band attributed to the sulfate half-esters was observed at 833 cm^{-1} and was the symmetric C–O–S vibration (Gu et al., 2010), which can be observed for CNCs (Fig. 4). In summary, based on results from the conductometric titration and FTIR spectroscopy analyses, we conclude that CNCs can be carboxylated by the selected LPMO9 while the carboxyl group content on the DeCNCs does not increase by modification using the LPMO9, and consequently they cannot be functionalized in the conditions studied.

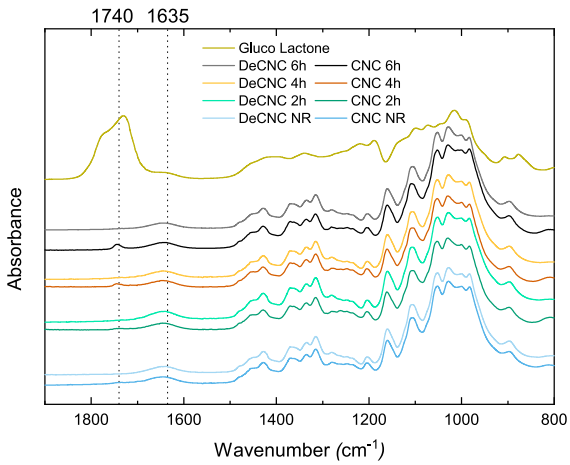

Fig. 4 ATR-FTIR spectra of CNCs (darker lines) and DeCNCs (lighter lines) reacted for 2, 4, and 6 h. Spectra of gluconolactone and controls without reductant (NR) after 6 h are shown. The 1635 cm^{-1} peak is attributed to the H–O–H bending vibration and hydrogen bonded hydroxy groups along with the absorbed water in carbohydrates. The band at 1745–1735 cm^{-1} is attributed to the C = O stretching associated with carboxylic acids

Colloidal stability of LPMO-modified CNC and DeCNC suspensions

The zeta-potential of the suspensions was analyzed to inspect alteration in the electrical double layer of the charged particles in water that is indicative of their colloidal stability. The zeta-potential values for all suspensions were lower (more negative) than −20 mV (Fig. 5), which indicates that all suspensions were colloidally stable since ±20–30 mV and > ±30 mV are moderately stable and highly stable, respectively (Bhattacharjee, 2016). We note that the zeta potential at which the systems achieve colloidal stability is associated with the point where the electrostatic potential overcomes the thermal energy. The higher values (less negative) for the DeCNCs, compared with the CNCs (−29.4 ± 0.4 mV vs. −37.5 ± 1.5 mV, respectively), support the observation that desulfation decreased the negatively charged sulfate half-ester group content.

The zeta-potential of the CNC suspension that was modified by applying LMPO9 for 6 h was −36 ± 3.0 mV. The zeta-potential of the control CNC NR was 37.5 ± 0.9 mV, similar to CNC NE (−37.5 ± 1.5 mV).

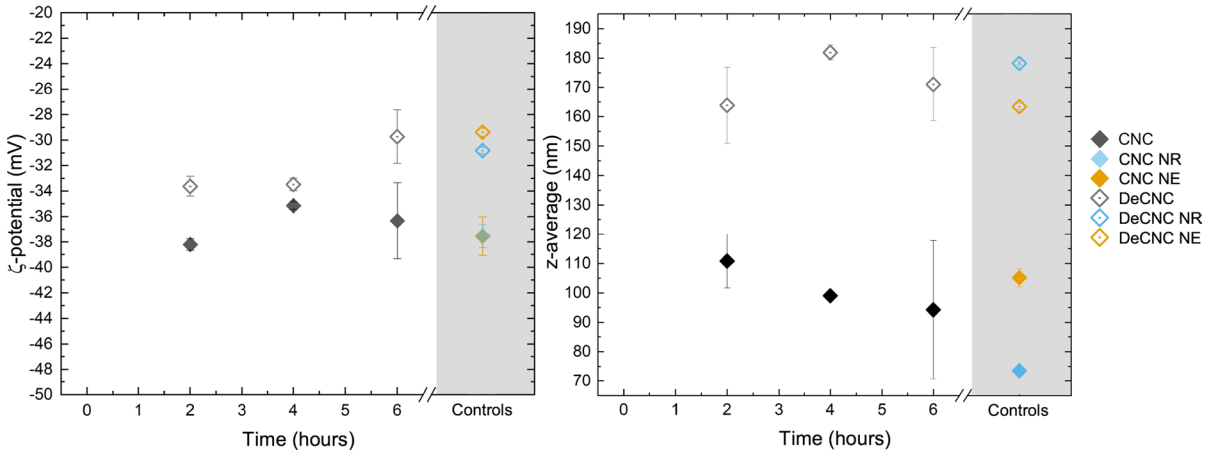

Fig. 5 Zeta-potential (left) and z-average (right) values of the LPMO-modified CNCs (♦) and DeCNCs (◇). Cellulose suspensions treated with LPMOs without reductant (NR) are indicated in blue, and those exposed to the reaction conditions without LPMOs are presented in yellow (NE). Controls were incubated for 6 h. The standard deviation represents the average of two reactions with at least six measurements. Note that two data points of DeCNC controls on the zeta-potential overlap on the left figure

The minute difference in the zeta-potential of CNCs that were enzymatically oxidized, compared with the controls, indicates that their colloidal stability was not altered. Karnaouri et al. (2020) also showed a slight increase in zeta-potential after post-treatment of sulfated tunicate CNCs with *Mt*LPMO9H.

The zeta-potential of DeCNC after 6 h LMPO9 oxidation was -29.7 ± 2.1 mV. The corresponding controls had almost unaltered zeta-potential values, at -30.9 ± 0.2 mV and -29.4 ± 0.4 mV for NR and NE control, respectively. The unaltered values of the zeta-potential suggest that the number of charged groups on the surface was not changed.

The CNC modification by LPMO modification could lead to a change in the space that the particles occupy in the suspension as a result of an increase or decrease in the surface charge or a decrease in the size of individual particles. This can be represented via hydrodynamic size, which is studied through the measure of z-average. The z-average is the intensity weighted mean hydrodynamic size of the ensemble collection of particles. The value of the particle size for CNCs represents an apparent particle size due to its rod-shaped form. The z-average will increase if the particles aggregate (Yeap et al., 2018).

The z-average was similar for all CNC suspensions: The mean z-average value was 97 nm. All DeCNC suspensions also had a similar mean z-average, at 172 nm. The mean z-average of DeCNCs was approximately 77% higher than the mean z-average of CNCs. The difference between the CNCs and DeCNCs indicates a higher aggregation tendency of the DeCNC suspensions. The aggregation was due to a decrease in the net charge indicated by the increased zeta-potential value (Fig. 5) that leads to a lowered electrosteric repulsion, and hence aggregation. The aggregation could decrease the accessibility of the enzyme to modify the surface. However, a larger fraction of solubilized oligomers than on the CNCs was detected on the DeCNCs (Fig. 2). The z-average values were not substantially different between the cellulose substrates modified using LPMOs and their controls, indicating that the modification did not change the z-average. In summary, the unchanged z-values are in line with the observation that the colloidal stability of the suspensions was maintained also after CNC modification by LPMO.

Sulfate half-ester and nitrogen content on the substrates

The sulfur content was determined to quantify the number of sulfate half-ester groups to verify that desulfation took place and to indirectly monitor the sulfate half-ester group content of LPMO-modified substrates with respect to the reaction time. CNC 6 h

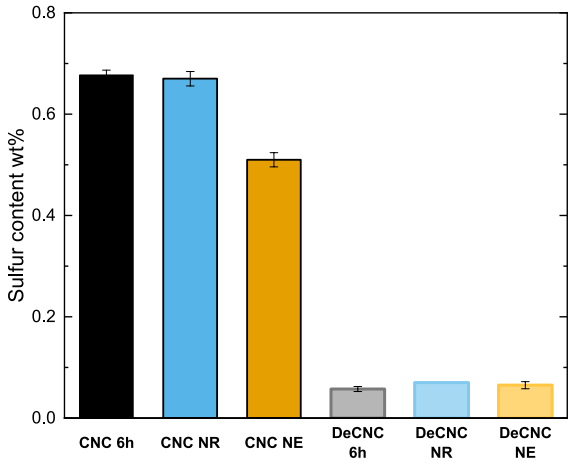

Fig. 6 Sulfur content (wt%) of CNCs and DeCNCs determined by elemental analysis after 6 h oxidation. NE and NR denote the control reactions that ran without the enzyme or without the reductant for 6 h, respectively

and CNC NR contained 0.67 ± 0.01 wt% and 0.66 ± 0.01 wt% sulfur, respectively, which was higher than the content in CNC NE, at 0.51 ± 0.01 wt% (Fig. 6). Since the sulfur content was at the same level for CNC 6 h and CNC NR control, it is possible to rely on the evaluation of carboxyl group content increase (Fig. 3), even if the CNC series had a higher carboxyl group content to begin with than the DeCNC series.

The modification of DeCNCs with LPMOs did not change the sulfur content as the sulfur content of DeCNC 6 h and DeCNC NR was 0.06 ± 0.01 wt% and 0.07 ± 0.01 wt%, respectively. The desulfation of CNCs to DeCNCs decreased the sulfur content of the NE controls from 0.51 ± 0.01 wt% to 0.07 ± 0.00 wt%. High-resolution XPS spectra of S2p confirmed that the CNC and DeCNC had a significant difference in sulfur content (Supporting Information Fig. S5). The desulfation technique using acids is known only to lead to partial desulfation (Jiang et al., 2010). The sulfur content analysis is contradictory to the findings by others where the sulfur content decreased with modification using *Mt*LPMO9H and *Pc*LPMO9D (Muraleedharan et al., 2021). However, different LPMOs at higher concentrations, higher temperatures, and longer reaction times were applied (Muraleedharan et al., 2021).

Nitrogen content was also analyzed (Supporting Information Fig. S2). An increase in the nitrogen content could be an indication that the LPMOs are adsorbed on the cellulose surfaces. It should be noted that the substrates were heated up to 100 °C and the pH was decreased to 2 where the enzyme was denatured. The denatured enzyme was folded in a random conformation that could adsorb stochastically to the surface of the cellulose substrates and thus the presence of nitrogen is only an indication that the enzyme was present as our analysis cannot distinguish if the enzyme adsorbed on the particles was denatured.

Morphology of oxidized cellulose substrates

The diameter of CNCs and DeCNCs (Fig. 7) prior to and after the oxidation was 3.7 and 5.7 nm, respectively, as estimated using analysis of AFM height profiles. Hence, the DeCNC diameter was 2 nm higher than the CNC diameter. The difference in diameter between the cellulose substrates can be explained by the aggregation of the crystals, which increases the difficulty to discern the individual particles (Llàcer Navarro et al., 2021). The challenge of identifying single particles is also evident from the high standard deviation. The crystallinity was also determined by XRD which remained non-altered during the CNC modification by the LPMO (Supporting Information Fig. S8).

A decrease in the diameter of the particles as a consequence of chemical modification is an indication of degradation (Llàcer Navarro et al. , 2021).

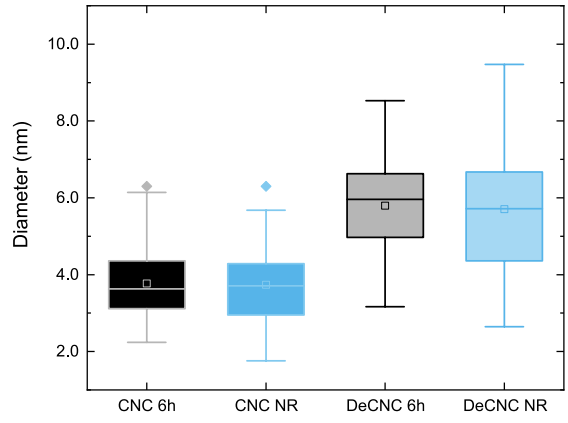

Fig. 7 Diameter of CNCs and DeCNCs determined using AFM height profiles. NR refers to the control condition where the enzyme was not activated with the reductant and 6 h to oxidation for 6 h. The rhombi represent the outliers, and the line and square inside the box are the median and the mean, respectively

The oxidation changed neither the DeCNC diameter nor that of the CNC (Fig. 7), indicating that the CNC modification by the LPMO did not degrade the particles (see also Supporting Information Fig. S7). Muraleedharan et al. (2021) and Karnaouri et al. (2020) reported a reduced diameter of CNCs and tunicin nanocrystals, respectively, as a result of LPMO activity, determined by AFM, and contradicting our findings. However, Solhi et al. (2022) indicated intact CNC morphology after the LPMO treatment. As pointed out above, such differences between studies are likely caused by the choice of the LPMO, analytics, and reaction conditions.

Coupling chemistry using the oxidized particles

The carboxyl groups that were introduced on the cellulose substrates using 6 h LPMO treatment were employed as linkers to connect the particles together, and for that, the EDC/NHS coupling chemistry with hexane-1,6-diamine was selected (Fig. 1b). First, EDC activates carboxyl groups and forms an amine-reactive O-acylisourea intermediate that spontaneously reacts with one of the amines of the hexane-1,6-diamine, and if the other part of the hexane-1,6-diamine finds an activated carboxyl group from another CNC, a crosslink may form. FTIR analysis of the systems revealed the presence of peaks at 1570 cm^{-1} and 3300 cm^{-1} in XCNC 6 h that were related to the secondary amides (C–N and C = O, respectively) introduced during the amidation reaction (Araki et al., 2015; Hase, 2004; Ma et al., 2017). The peak at 1570 cm^{-1} was related to the −N(H)–C = O bond, and that at 3300 cm^{-1} was related to the C–N vibration (Fig. 8). The peak at 1745–1735 cm^{-1} was attributed to the C = O stretching associated with carboxylic acids. The peak at 1745–1735 cm^{-1} disappeared with amidation, demonstrating that the carboxyl groups were consumed during the reaction.

The sulfur content of CNCs and DeCNCs was not significantly altered with the amidation reaction (Supporting Information Figs. S6 and S5). The amount of nitrogen was also determined (Supporting Information Fig. S3). However, since the enzyme and the amidated substances contain nitrogen, the analysis cannot be used for the evaluation.

The z-average of the crosslinked CNCs and DeCNCs was determined to assess the relative degree of crosslinking. The highest z-average value (Fig. 9)

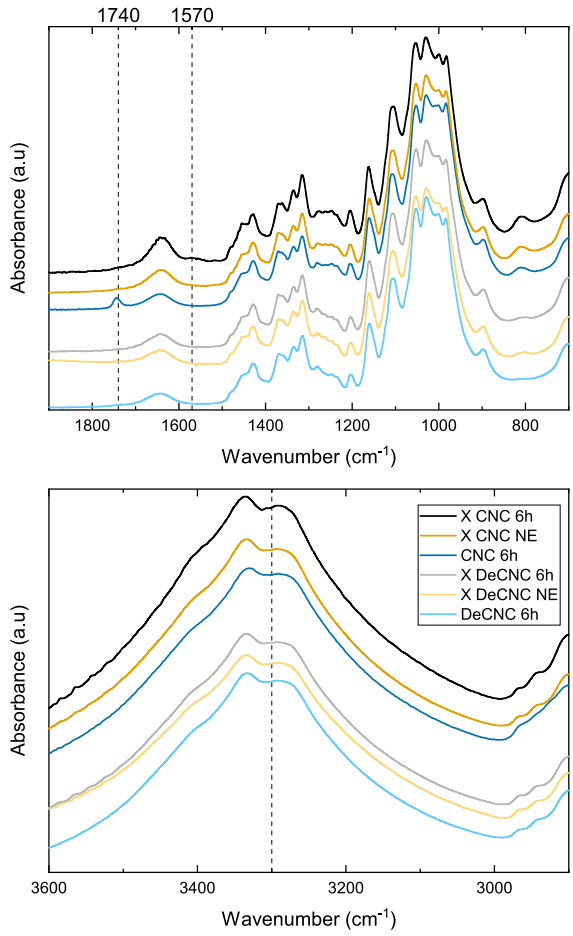

Fig. 8 **a** ATR-FTIR spectra from 1900 to 700 cm^{-1} and **b** 3600 to 3000 cm^{-1} of the LPMO-modified CNCs (darker line) and DeCNCs (lighter lines). Crosslinked modified cellulose substrates (XCNC 6 h and XDeCNC 6 h), crosslinked unmodified cellulose substrates (XCNC NE and XDeCNC NE) and non-crosslinked cellulose LPMO after 6 h (CNC 6 h and DeCNC 6 h) are shown. The bands of interest (black dashed lines) at 1570 cm^{-1} and 3300 cm^{-1} are related to the presence of secondary amides (N–H and C = O, respectively). The band of interest at 1745–1735 cm^{-1} is attributed to the C = O stretching associated with carboxylic acids

286 ± 2 nm was recorded for the amidated CNC 6 h suspension (XCNC 6 h), presenting dispersity of 1 (in a scale of 0 to 1). The dispersity shown by XCNC 6 h indicates a broad size distribution of the particle because the CNCs were crosslinked forming differently sized crosslinked CNCs. The z-average was three times higher than before amidation (CNC 6 h). Ellebracht and Jones (2018) used a similar method to amidate TEMPO-oxidized DeCNCs with

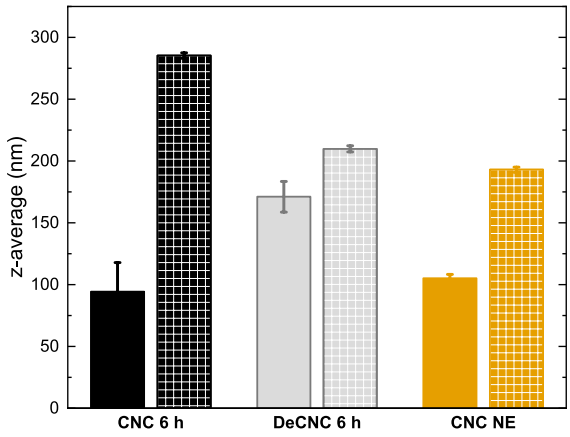

Fig. 9 Z-average values of the LPMO-modified CNCs and DeCNCs (6 h reaction time) before (solid pattern) and after amidation reaction (sparse pattern) determined by DLS. Cellulose suspensions treated with LPMOs without enzyme (NE) for 6 h before and after amidation are shown. The standard deviation represents 3 measurements

hexane-1,6-diamine and analyzed the products with DLS. The hydrodynamic radius of the amidated DeCNC was four times higher with a larger distribution than the control. Controls of amidated CNC NE (XCNC NE) displayed dispersity of 0.3 and a z-average of 192 ± 2 nm, which was 1.8 times higher than before amidation (CNC NE), thereby indicating that exposing the system to the reaction condition leads to an increase in the z-average (and hence indirectly indicating clustering of the particles). The DeCNC 6 h suspension that was amidated (XDeCNC 6 h) displayed a z-average of 210 ± 3 nm, which was 1.2 times higher than before amidation, and a dispersity of 0.15. The increase in z-average is surprising since the carboxyl group content was low (Fig. 3). However, the change in z-average values using the LPMO-modified CNCs was higher that using the control CNCs, and higher than for the DeCNCs, and hence is in line with LPMO treatment of CNCs leading to the addition of carboxyl groups that enable the coupling chemistry.

In summary, the FTIR of the XCNC 6 h (Fig. 8) confirmed the presence of C–N and C = O at 1570 cm^{-1} and 3300 cm^{-1} and the disappearance of the peak representing the carboxyl group at 1740 cm^{-1}. Also, the increase of nitrogen, determined by XPS, and increase of z-average, determined by the DLS, suggested that the XCNC 6 h was successfully amidated and crosslinked to some extent proving that the LPMO oxidation enables the crosslinking.

Conclusions

The carboxylation of sulfated CNCs using the *Tt*LPMO9G presented here is mild and non-destructive. The LPMO was found to be active on both cellulose substrates that were studied, namely sulfated CNCs and desulfated CNCs (CNCs and DeCNCs). CNC modification by LPMO increased the number of carboxyl groups (10%) only on sulfated CNCs. This increase in carboxyl group content allowed the demonstration of coupling chemistry using EDC/NHS and hexane-1,6-diamine. The sulfate half-ester groups played an important role in the CNC modification by the LPMO as more solubilized oligosaccharides were found when the DeCNC substrate was used, whereas the CNC substrate was surface modified to a higher degree than the DeCNC. The results of this research underline the relevance of analyzing both solid and soluble LPMO reaction products as a combinatory methodology to access conclusions of LPMO activity on solid substrates.

Here, it is suggested that the sulfate half-ester groups hinder the adsorption of the LPMO and decrease the probability that the enzymes are able to attack a cellulose chain at positions that are a few anhydroglucose units apart and consequently, this inhibits the solubilization of that part of the chain. The LPMOs oxidized CNCs increasing the carboxyl groups without a change in the particle diameter or colloidal stability. The sulfur content before and after the LPMO treatment remained constant, which indicates that the sulfate groups are not affected by the modification and hence remain for follow-up use and facilitating colloidal stability.

The amidation of the enzymatically oxidized CNCs led to the appearance of new peaks in FTIR spectroscopy analysis related to the presence of secondary amines. Also, the increase of the z-average of the amidated cellulose substrates indicated that not only the coupling chemistry reaction took place but also the particles crosslinked. The 3-fold increase of z-average of the enzymatically modified CNC after 6 h revealed that the LPMO had a decisive role in producing the addition of carboxyl available groups.

Acknowledgments Prof. Vincent Eijsink at the Norwegian University of Life Sciences is thanked for LPMO-related discussions. Dr. Andreas Schaefer is thanked for the X-ray scattering. The Chalmers Material Analysis Laboratory (CMAL) is acknowledged for providing access to the XRD, as is Dr. Michal Strach for the XRD measurements. Professor Johan Bergenholtz at the University of Gothenburg is thanked for access to the zeta-potential and z-average measurements. Figure 1 was created with BioRender.com.

Author Contributions S.L.N. and M.T. performed the experimental work and data analysis with focus on the cellulose substrate and the enzymes, respectively. S.L.N. and M.T. wrote the first draft of the manuscript. S.L.N. and M.T contributed equally. L.O. and T.N. were responsible of conceptualization and supervision. All authors edited and reviewed the manuscript.

Funding Open access funding provided by Chalmers University of Technology. The work was performed at the Wallenberg Wood Science center funded by the Knut and Alice Wallenberg Foundation and the Chalmers Foundation.

Data availability Data will be made available upon request.

Declarations

Conflict of interest The authors declare that they have no conflict of interest or competing interest.

References

Agger JW, Isaksen T, Várnai A, Vidal-Melgosa S, Willats WG, Ludwig R, Horn SJ, Eijsink VG, Westereng B (2014) Discovery of LPMO activity on hemicelluloses shows the importance of oxidative processes in plant cell wall degradation. Proc Natl Acad Sci 111(17):6287–6292

Akhlaghi SP, Berry RC, Tam KC (2013) Surface modification of cellulose nanocrystal with chitosan oligosaccharide for drug delivery applications. Cellulose 20(4):1747–1764

Akhlaghi SP, Tiong D, Berry RM, Tam KC (2014) Comparative release studies of two cationic model drugs from different cellulose nanocrystal derivatives. Eur J Pharm Biopharm 88(1):207–215

Araki K, Yagi N, Ikemoto Y, Yagi H, Choong CJ, Hayakawa H, Beck G, Sumi H, Fujimura H, Moriwaki T, Nagai Y, Goto Y, Mochizuki H (2015) Synchrotron FTIR microspectroscopy for structural analysis of Lewy bodies in the brain of Parkinson's disease patients. Sci Rep 5(1):17625. https://doi.org/10.1038/srep17625

Arcot LR, Lundahl M, Rojas OJ, Laine J (2014) Asymmetric cellulose nanocrystals: thiolation of reducing end groups via NHS-EDC coupling. Cellulose 21(6):4209–4218. https://doi.org/10.1007/s10570-014-0426-9

Bennati-Granier C, Garajova S, Champion C, Grisel S, Haon M, Zhou S, Fanuel M, Ropartz D, Rogniaux H, Gimbert I et al (2015) Substrate specificity and regioselectivity of fungal AA9 lytic polysaccharide monooxygenases secreted by Podospora anserina. Biotechnol Biofuels 8(1):1–14

Bhattacharjee S (2016) Dls and zeta potential - what they are and what they are not? J Controll Releas 235:337–351. https://doi.org/10.1016/j.jconrel.2016.06.017

Bissaro B, Røhr ÅK, Müller G, Chylenski P, Skaugen M, Forsberg Z, Horn SJ, Vaaje-Kolstad G, Eijsink VG (2017) Oxidative cleavage of polysaccharides by monocopper enzymes depends on H_2O_2. Nat Chem Biol 13(10):1123–1128

Chalak A, Villares A, Moreau C, Haon M, Grisel S, d'Orlando A, Herpoël-Gimbert I, Labourel A, Cathala B, Berrin JG (2019) Influence of the carbohydrate-binding module on the activity of a fungal AA9 lytic polysaccharide monooxygenase on cellulosic substrates. Biotechnol biofuels 12(1):1–10

Chen C, Chen J, Geng Z, Wang M, Liu N, Li D (2018) Regioselectivity of oxidation by a polysaccharide monooxygenase from Chaetomium thermophilum. Biotechnol Biofuels 11(1):1–16

Chorozian K, Karnaouri A, Karantonis A, Souli M, Topakas E (2022) Characterization of a dual cellulolytic/xylanolytic aa9 lytic polysaccharide monooxygenase from thermothelomyces thermophilus and its utilization toward nanocellulose production in a multi-step bioprocess. ACS Sustain Chem Eng 10(27):8919–8929

Chylenski P, Bissaro B, Sørlie M, Røhr ÅK, Varnai A, Horn SJ, Eijsink VG (2019) Lytic polysaccharide monooxygenases in enzymatic processing of lignocellulosic biomass. ACS Catal 9(6):4970–4991

Courtade G, Forsberg Z, Heggset EB, Eijsink VG, Aachmann FL (2018) The carbohydrate-binding module and linker of a modular lytic polysaccharide monooxygenase promote localized cellulose oxidation. J Biological Chem 293(34):13006–13015. https://doi.org/10.1074/jbc.RA118.004269

Delepierre G, Vanderfleet OM, Niinivaara E, Zakani B, Cranston ED (2021) Benchmarking cellulose nanocrystals part II: new industrially produced materials. Langmuir 37(28):8393–8409. https://doi.org/10.1021/acs.langmuir.1c00550

Drula E, Garron ML, Dogan S, Lombard V, Henrissat B, Terrapon N (2022) The carbohydrate-active enzyme database: functions and literature. Nucl Acids Res 50(D1):D571–D577

Dufresne A (2013) Nanocellulose: a new ageless bionanomaterial. Mater Today 16(6):220–227. https://doi.org/10.1016/j.mattod.2013.06.004

Ehmann HM, Mohan T, Koshanskaya M, Scheicher S, Breitwieser D, Ribitsch V, Stana-Kleinschek K, Spirk S (2014) Design of anticoagulant surfaces based on cellulose nanocrystals. Chem Commun 50(86):13070–13072

Eibinger M, Sattelkow J, Ganner T, Plank H, Nidetzky B (2017) Single-molecule study of oxidative enzymatic deconstruction of cellulose. Nat Commun 8(1):1–7

Ellebracht NC, Jones CW (2018) Amine functionalization of cellulose nanocrystals for acid-base organocatalysis: surface chemistry, cross-linking, and solvent effects. Cellulose 25(11):6495–6512. https://doi.org/10.1007/s10570-018-2043-5

Foster EJ, Moon RJ, Agarwal UP, Bortner MJ, Bras J, Camarero-Espinosa S, Chan KJ, Clift MJD, Cranston ED, Eichhorn SJ, Fox DM, Hamad WY, Heux L, Jean B, Korey M, Nieh W, Ong KJ, Reid MS, Renneckar S, Roberts R, Shatkin JA, Simonsen J, Stinson-Bagby K, Wanasekara N, Youngblood J (2018) Current characterization methods for cellulose nanomaterials. Chem Soc Rev 47(8):2609–2679. https://doi.org/10.1039/C6CS00895J

Frandsen KE, Haon M, Grisel S, Henrissat B, Leggio LL, Berrin JG (2021) Identification of the molecular determinants driving the substrate specificity of fungal lytic polysaccharide monooxygenases (LPMOs). J Biol Chem 296

Fraschini C, Chauve G, Bouchard J (2017) TEMPO-mediated surface oxidation of cellulose nanocrystals (CNCs). Cellulose 24(7):2775–2790. https://doi.org/10.1007/s10570-017-1319-5

French AD (2014) Idealized powder diffraction patterns for cellulose polymorphs. Cellulose 21(2):885–896. https://doi.org/10.1007/s10570-013-0030-4

Frommhagen M, Sforza S, Westphal AH, Visser J, Hinz SW, Koetsier MJ, van Berkel WJ, Gruppen H, Kabel MA (2015) Discovery of the combined oxidative cleavage of plant xylan and cellulose by a new fungal polysaccharide monooxygenase. Biotechnol Biofuels 8(1):1–12

Gu J, Catchmark JM, Archibald DD, Kaiser EQ (2010) Determination of sulfate esterification levels in cellulose nanocrystals by attenuated total reflectance - Fourier transform infrared spectroscopy. Am Soc Agric Biol Eng Ann Int Meet ASABE 1(10):23–32

Habibi Y, Lucia LA, Rojas OJ (2010) Cellulose nanocrystals: chemistry, self-assembly, and applications. Chem Rev 110(6):3479–3500

Hase T (2004) Tables for organic spectrometry. Otatieto, Helsinki. ISBN 978-951-672-276-7

Hu J, Tian D, Renneckar S, Saddler JN (2018) Enzyme mediated nanofibrillation of cellulose by the synergistic actions of an endoglucanase, lytic polysaccharide monooxygenase (LPMO) and xylanase. Sci Rep 8(1):1–8

Hüttner S, Várnai A, Petrović DM, Bach CX, Kim Anh DT, Thanh VN, Eijsink VG, Larsbrink J, Olsson L (2019) Specific xylan activity revealed for AA9 lytic polysaccharide monooxygenases of the thermophilic fungus Malbranchea cinnamomea by functional characterization. Appl Environ Microbiol 85(23):e01408-19

Isogai A, Saito T, Fukuzumi H (2011) TEMPO-oxidized cellulose nanofibers. Nanoscale 3(1):71–85

Ji H, Xiang Z, Qi H, Han T, Pranovich A, Song T (2019) Strategy towards one-step preparation of carboxylic cellulose nanocrystals and nanofibrils with high yield, carboxylation and highly stable dispersibility using innocuous citric acid. Green Chem 21(8):1956–1964

Jiang F, Esker AR, Roman M (2010) Acid-catalyzed and solvolytic desulfation of H_2SO_4-hydrolyzed cellulose nanocrystals. Langmuir 26(23):17919–17925. https://doi.org/10.1021/la1028405

Jiang F, Kittle JD, Tan X, Esker AR, Roman M (2013) Effects of sulfate groups on the adsorption and activity of cellulases on cellulose substrates. Langmuir 29(10):3280–91. https://doi.org/10.1021/la3040193

Karnaouri A, Jalvo B, Moritz P, Matsakas L, Rova U, Hofft O, Sourkouni G, Maus-Friedrichs W, Mathew AP, Christakopoulos P (2020) Lytic polysaccharide monooxygenase-assisted preparation of oxidized-cellulose nanocrystals with a high carboxyl content from the tunic of marine invertebrate Ciona intestinalis. ACS Sustain Chem Eng 8(50):18400–18412

Koskela S, Wang S, Xu D, Yang X, Li K, Berglund LA, McKee LS, Bulone V, Zhou Q (2019) Lytic polysaccharide monooxygenase (LPMO) mediated production of ultra-fine cellulose nanofibres from delignified softwood fibres. Green Chem 21(21):5924–5933

Koskela S, Wang S, Fowler PMP, Tan F, Zhou Q (2021) Structure and self-assembly of lytic polysaccharide monooxygenase-oxidized cellulose nanocrystals. ACS Sustain Chem Eng 9(34):11331–11341. https://doi.org/10.1021/acssuschemeng.1c02407

Llàcer Navarro S, Nakayama K, Idström A, Evenäs L, Ström A, Nypelö T (2021) The effect of sulfate half-ester groups on cellulose nanocrystal periodate oxidation. Cellulose 28(15):9633–9644

Ma H, Wang S, Meng F, Xu X, Huo X (2017) A hydrazone-carboxyl ligand-linked cellulose nanocrystal aerogel with high elasticity and fast oil/water separation. Cellulose 24(2):797–809. https://doi.org/10.1007/s10570-016-1132-6

Magri S, Nazerian G, Segato T, Monclaro AV, Zarattini M, Segato F, Polikarpov I, Cannella D (2022) Polymer ultrastructure governs AA9 lytic polysaccharide monooxygenases functionalization and deconstruction efficacy on cellulose nano-crystals. Bioresour Technol 347:126375

Marchessault R, Morehead F, Koch M (1961) Some hydrodynamic properties of neutral suspensions of cellulose crystallites as related to size and shape. J Coll Sci 16(4):327–344. https://doi.org/10.1016/0095-8522(61)90033-2

Marchessault RH, Morehead FF, Walter NM (1959) Liquid crystal systems from fibrillar polysaccharides. Nature 184(4686):632–633. https://doi.org/10.1038/184632a0

Marjamaa K, Rahikainen J, Karjalainen M, Maiorova N, Holopainen-Mantila U, Molinier M, Aro N, Nygren H, Mikkelson A, Koivula A, et al. (2022) Oxidative modification of cellulosic fibres by lytic polysaccharide monooxygenase AA9A from *Trichoderma reesei*. Cellulose pp 1–18

Moreau C, Tapin-Lingua S, Grisel S, Gimbert I, Le Gall S, Meyer V, Petit-Conil M, Berrin JG, Cathala B, Villares A (2019) Lytic polysaccharide monooxygenases (LPMOs)

facilitate cellulose nanofibrils production. Biotechnol Biofuels 12(1):1–13

Muraleedharan MN, Karnaouri A, Piatkova M, Ruiz-Caldas MX, Matsakas L, Liu B, Rova U, Christakopoulos P, Mathew AP (2021) Isolation and modification of nanoscale cellulose from organosolv-treated birch through the synergistic activity of LPMO and endoglucanases. Int J Biol Macromol 183:101–109. https://doi.org/10.1016/J.IJBIOMAC.2021.04.136

Nypelö T, Amer H, Konnerth J, Potthast A, Rosenau T (2018) Self-standing nanocellulose janus-type films with aldehyde and carboxyl functionalities. Biomacromolecules 19(3):973–979. https://doi.org/10.1021/acs.biomac.7b01751

Petrović DM, Várnai A, Dimarogona M, Mathiesen G, Sandgren M, Westereng B, Eijsink VG (2019) Comparison of three seemingly similar lytic polysaccharide monooxygenases from Neurospora crassa suggests different roles in plant biomass degradation. J Biol Chem 294(41):15068–15081

Quinlan RJ, Sweeney MD, Lo Leggio L, Otten H, Poulsen JCN, Johansen KS, Krogh KB, Jørgensen CI, Tovborg M, Anthonsen A et al (2011) Insights into the oxidative degradation of cellulose by a copper metalloenzyme that exploits biomass components. Proc Natl Acad Sci 108(37):15079–15084

Rånby BG (1951) Fibrous macromolecular systems. cellulose and muscle. the colloidal properties of cellulose micelles. Discussions Faraday Soc 11:158–164

Revol JF, Bradford H, Giasson J, Marchessault R, Gray D (1992) Helicoidal self-ordering of cellulose microfibrils in aqueous suspension. Int J Biol Macromol 14(3):170–172. https://doi.org/10.1016/S0141-8130(05)80008-X

Rossi BR, Pellegrini VO, Cortez AA, Chiromito EM, Carvalho AJ, Pinto LO, Rezende CA, Mastelaro VR, Polikarpov I (2021) Cellulose nanofibers production using a set of recombinant enzymes. Carbohydr Polym 256:117510

Solhi L, Li J, Li J, Heyns NMI, Brumer H (2022) Oxidative enzyme activation of cellulose substrates for surface modification. Green Chem 24:4026–4040. https://doi.org/10.1039/D2GC00393G

Sun P, Laurent CV, Boerkamp VJ, van Erven G, Ludwig R, van Berkel WJ, Kabel MA (2022) Regioselective C4 and C6 double oxidation of cellulose by lytic polysaccharide monooxygenases. ChemSusChem 15(2):e202102203

Tõlgo M, Hegnar OA, Østby H, Várnai A, Vilaplana F, Eijsink VG, Olsson L (2022) Comparison of six lytic polysaccharide monooxygenases from thermothielavioides terrestris shows that functional variation underlies the multiplicity of LPMO genes in filamentous fungi. Appl Environ Microbiol 88(6):e00096-22

Vaaje-Kolstad G, Westereng B, Horn SJ, Liu Z, Zhai H, Sørlie M, Eijsink VG (2010) An oxidative enzyme boosting the enzymatic conversion of recalcitrant polysaccharides. Science 330(6001):219–222

Villares A, Moreau C, Bennati-Granier C, Garajova S, Foucat L, Falourd X, Saake B, Berrin JG, Cathala B (2017) Lytic polysaccharide monooxygenases disrupt the cellulose fibers structure. Sci Rep 7(1):1–9

Vu VV, Beeson WT, Phillips CM, Cate JH, Marletta MA (2014) Determinants of regioselective hydroxylation in the fungal polysaccharide monooxygenases. J Am Chem Soc 136(2):562–565

Wang D, Li J, Salazar-Alvarez G, McKee LS, Srivastava V, Sellberg JA, Bulone V, Hsieh YS (2018) Production of functionalised chitins assisted by fungal lytic polysaccharide monooxygenase. Green Chem 20(9):2091–2100

Wang H, Qian C, Roman M (2011) Effects of pH and salt concentration on the formation and properties of chitosan-cellulose nanocrystal polyelectrolyte-macroion complexes. Biomacromolecules 12(10):3708–3714. https://doi.org/10.1021/bm2009685

Yeap SP, Lim J, Ngang HP, Ooi BS, Ahmad AL (2018) Role of particle-particle interaction towards effective interpretation of Z-average and particle size distributions from dynamic light scattering (DLS) analysis. J Nanosci Nanotechnol 18(10):6957–6964. https://doi.org/10.1166/jnn.2018.15458

Zhang S, Li J, Chen S, Zhang X, Ma J, He J (2020) Oxidized cellulose-based hemostatic materials. Carbohydr Polym 230:115585